

**PREPRINT SUBMITTED NOT PEER-REVIEWED**

This manuscript is a **preprint** uploaded to **EarthArXiv**. It has been **submitted** for publication to **Earth and Planetary Science Letters (EPSL)** on the **26/09/2019**. This preprint version of the manuscript **has not** undergone **peer-review**. Newer versions may be moderately different with slight variations in content. Authors encourage downloading the latest manuscript version from EarthArXiv before usage. Authors welcome feedback, discussion and comments anytime. For comments, you can use hypothes.is (<https://web.hypothes.is/>).

Feel free to get in contact: [geo.david.fernandez@gmail.com](mailto:geo.david.fernandez@gmail.com)

# Forearc high uplift by deep crustal flow during growth of the Anatolian margin

**David Fernández-Blanco<sup>1</sup>, Utsav Mannu<sup>2,3</sup>, Giovanni Bertotti<sup>1</sup>, and Sean D. Willett<sup>4</sup>**

<sup>1</sup> Department of Geoscience and Engineering, Faculty of Civil Engineering and Geosciences, Delft, University of Technology, Stevinweg 1, 2628CN, Delft, the Netherlands, [geo.david.fernandez@gmail.com](mailto:geo.david.fernandez@gmail.com)

<sup>2</sup> Earthquake and Volcano Information, Earthquake Research Institute, Tokyo University.

<sup>3</sup> Department of Earth & Climate, Indian Institute of Science Education and Research, Pune.

<sup>4</sup> Geological Institute, Swiss Federal Institute of Technology, 8092 Zurich, Switzerland.

## Abstract

We present a model for the dynamic formation of the forearc high of southern Anatolia where sedimentation in the forearc basin leads to thermally-activated deformation in the lower crust. Our thermo-mechanical models demonstrate that forearc sedimentation increases the temperature of the underlying crust by “blanketing” the heat flux and increasing Moho depth. Deformation switches from frictional to viscous with a higher strain rate led by increased temperature. Viscous deformation changes large-wavelength subsidence into coeval, short-wavelength uplift and subsidence. Models show that forearc highs are intrinsic to accretionary wedges and can grow dynamically and non-linearly at rates dependent on sediment accretion, sedimentation and temperature. The mechanism explains Neogene first-order upper-plate strain and vertical motions in the Anatolian margin along Central Cyprus, and in the orogenic plateau margin in South Turkey. This system is analogous to forearc highs in other mature accretionary margins, like Cascadia, Lesser Antilles or Nankai.

**keywords:** forearc high; plateau margin; subduction zone; subduction wedge; uplift; Central Anatolian Plateau

## **Manuscript highlights**

Models show a mechanism where forearc sediments thermally activate deep crustal flow

Viscous flow changes regional subsidence into short-wavelength uplift/subsidence

Forearc high uplift is controlled by sediment accretion, sedimentation and temperature

Mechanism explains S Anatolia upper-plate strain and vertical motions in Neogene

Mechanism explains S Turkey uplift by accretion and viscous flow, not slab break-off

## **1 Introduction**

Climatic and geodynamic processes are the first-order drivers of topography in orogenic plateaus and plateau margins. However, mechanisms for detailed patterns of uplift in orogenic plateau systems, such as Himalaya-Tibet and Puna-Altiplano (e.g., Allmendinger et al., 1997; Molnar, 1984) remain diverse and difficult to generalize. This is also true for the history of topography growth of the orogenic plateau of Central Anatolia and its margins. While continental delamination (Bartol and Govers, 2014) or lithospheric drip (Göğüş et al., 2017) have been suggested to sustain Central Anatolia low relief at ~1 km, its plateau margins are geodynamically different; transpressional orogenic uplift may have formed the northern margin (Yildirim et al., 2011) whereas the southern margin is strongly influenced by the Cyprus subduction zone to the south. The formation mechanism of the latter is of particular interest, for the uplift in the southern margin has a limited N-S extent and occurred in the absence of regional accommodating faults (Fernández-Blanco et al., 2019).

The southern margin of the Central Anatolian Plateau (SCAP) (Fig. 1) is suggested to form by shallow break-off of the Cyprus slab (e.g., Schildgen et al., 2014). This geodynamic scenario is compatible with stratigraphic and paleontological records (Cosentino et al., 2012) and the thinned Central Anatolian lithosphere inferred from seismic tomography (Mutlu and Karabulut, 2011). However, the presence of the African slab (e.g., Abgarmi et al., 2017) and the thick Anatolian mantle lithosphere (Delph et al., 2017) under the modern Central Taurides suggest that this mechanism is not likely to be active over the entire E-W extent of the Taurides. In addition, the large wavelength motions expected at the surface during slab break-off (e.g., Göğüş and Pysklywec, 2008) are at odds with the sharp bound and short wavelength between margin uplift and seaward subsidence in South Turkey (Fernández-Blanco et al., 2019; Walsh-Kennedy et al., 2014). Therefore, we ought to look for other causal mechanisms, such as crustal thickening, to explain the elevation of the plateau margin (Fernández-Blanco, 2014; Fernández-Blanco et al., 2019; Meijers et al., 2018).

Forearc deformation of an orogenic wedge (Platt, 1986; Willett et al. 1993), where deep-seated crustal flow results in forearc high uplift has been proposed as a general mechanism for forearc uplift with examples from the Lesser Antilles, Cascadia and other accretionary margins (e.g., Pavlis and Bruhn, 1983; Williams et al., 1994). The development of a preceding forearc basin that is later fragmented by the uplift of the high (McNeill et al., 2000) has been suggested in more detailed mechanical models. If the forearc basin forms as a negative-alpha basin, stabilizing the underlying wedge (Willett & Schlunegger, 2010), basin growth may promote ductile deformation in the lower crust, and a later stage, uplift of the forearc high (Fuller et al., 2006). We demonstrate that the mechanism of deep crustal thickening by thermally-activated viscous flow, as proposed by Fuller et al. (2006) and expanded here, reproduces the first-order spatiotemporal pattern of deformation and vertical motion (uplift and subsidence) across the SCAP during its growth as the forearc high of the Central Cyprus forearc.

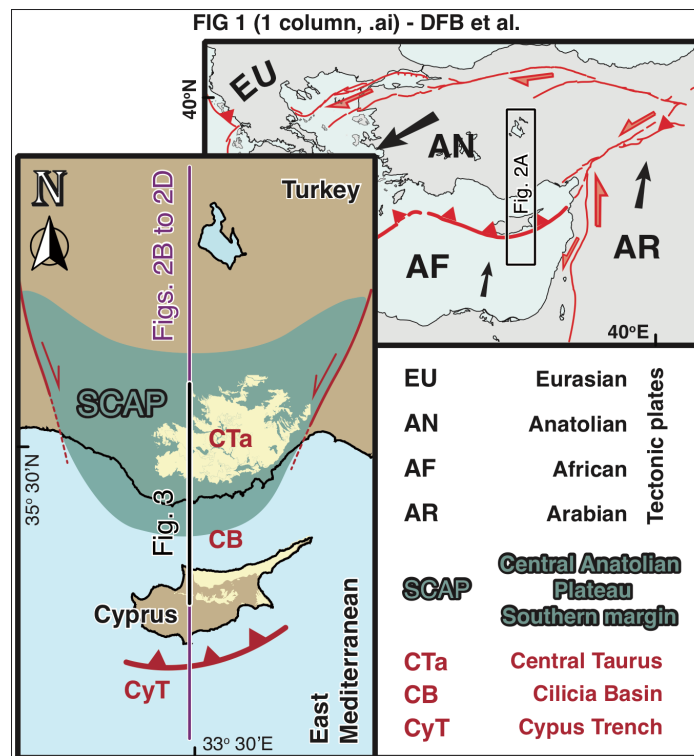


**Figure 1.** Central Cyprus subduction zone and its surrounding tectonic frame, with the location of transects in figures 2 and 3. Neogene rocks on Central Taurides and Cyprus are in yellow. EU, AN, AF and AR = Eurasian, Anatolian, African and Arabian tectonic plates; SCAP = Southern margin of the Central Anatolian Plateau; CTa = Central Taurides; CB = Cilicia Basin; CyT = Cyprus trench.

Here, we explore the role of wedge-top sedimentation on forearc dynamics for conditions applicable to the Cyprus-Anatolia margin. To do this, we use transects of the Central Cyprus subduction margin and its forearc, derived by integration of geophysical and geological data, to constraint coupled thermo-mechanical, visco-plastic numerical models. An important transition emerges in these models as accretionary growth and sediment deposition produce a “thermal blanketing” effect restricting heat flux from underneath the forearc basin and leading to thermal weakening of the upper plate. In this context, a forearc high grows dynamically and non-linearly as an integral part of an accreting wedge, often seaward of any continental backstop. This thermo-mechanical interplay can provide an important uplift mechanism applicable to the Anatolian margin that can be generalised to similar accretionary margins.

## **2 Background**

The Africa/Arabia-Eurasian plate convergence and subduction dynamics that dominate the Mediterranean controls the evolution of the Anatolian margin (Wortel and Spakman, 2000), where the SCAP occupies the forearc high of the Central Cyprus subduction at present (Fig. 1). Early to Late Miocene subsidence broadened a wide forearc basin that spanned from South Turkey to Central Cyprus, and led to protracted growth of a laterally continuous carbonate platform (e.g., Bassant et al., 2005; Karabiyikoğlu et al., 2000). Late Miocene regional vertical motions of short wavelength and opposite sense led to coeval South Turkey uplift and seaward subsidence (Walsh-Kennedy et al., 2014). These short-wavelength motions of opposite sense fragmented the antecedent forearc basin while forming the SCAP as a flexural monocline absent of regional surface-reaching faults (Fernández-Blanco et al., 2019). The vertical motions led to truncation and erosion of Late Miocene rocks in the uplifting sectors of the SCAP while subsiding sectors of the monocline sustained deposition, leading to maximum sediment thicknesses near the Turkish coast (Aksu et al., 2005; Walsh-Kennedy et al., 2014). At present, the monocline is delineated by Late Miocene shallow marine rocks laying at ~2 km elevation in the modern Central Taurides (Cosentino et al., 2012) and at ~-2 km depth in the Cilicia Basin

(Aksu et al., 2005).

Mutually contradictory evidence along the plateau margin keeps open the debate on when and how it was formed. Biostratigraphy and polarity chrons report an age of 8.35–8.108 Ma for marine rocks at the top of the sequence in the present-day Central Taurides hinterland (Cosentino et al., 2012). The lateral continuity of these marine rocks across the plateau margin and their contact relationships with the basement, together with the absence of Messinian deposits, suggest km-scale topography by >5 Ma (Fernández-Blanco et al., 2019). This is consistent with stable isotope paleoaltimetry estimates pointing at ~2 km of relief at ~5 Ma (Meijers et al., 2018), and the protracted sedimentary deposition in thick, stacked delta lobes in the Göksu Delta during latest Messinian - Recent seen in seismic reflection lines (Aksu et al., 2014). Cosmogenic datation of Göksu River terraces and uplifted marine fossil assemblages suggest surface uplift onset between 8 and 5.45 Ma with average uplift rates of 0.25 to 0.37 mm/yr, and uplift rates of 0.72 to 0.74 mm/yr leading to 1.2 km of surface uplift since 1.66 to 1.62 Ma (Schildgen et al., 2012). Paleontological evidence in younger marine rocks at the margins of the Göksu River or closer to the coast points to uplift rates as fast as 3.21-3.42 mm/yr and suggests 1200-1500 m of topographic growth in the last ~450 ka (Öğretmen et al., 2018).

Studies using the ages of onshore uplifted features as markers of different phases of uplift suggest the SCAP formed by delamination and/or slab break-off events that vary in time and/or depth (e.g., Cosentino et al., 2012; Öğretmen et al., 2018; Schildgen et al., 2014, 2012). However, these studies constrain depositional age or subaerial exposure of rocks at specific sites, and the proposed geodynamic scenarios of multiple uplift phases overlook the presence of the African slab below the modern Central Taurides and the relevant thickness of the Anatolian crust and lithosphere there (e.g., Abgarmi et al., 2017; Bakırcı et al., 2012; Biryol et al., 2011; Delph et al., 2017). Studies accounting for aforementioned geological constraints and geophysical observables suggest crustal thickening as an alternative mechanism of plateau margin formation (Fernández-Blanco, 2014; Fernández-Blanco et al., 2019; Meijers et al., 2018). Yet,

these latter studies seem to be at odds with the youngest uplifted marine rocks and provide no detail on the mechanism leading to crustal thickening.

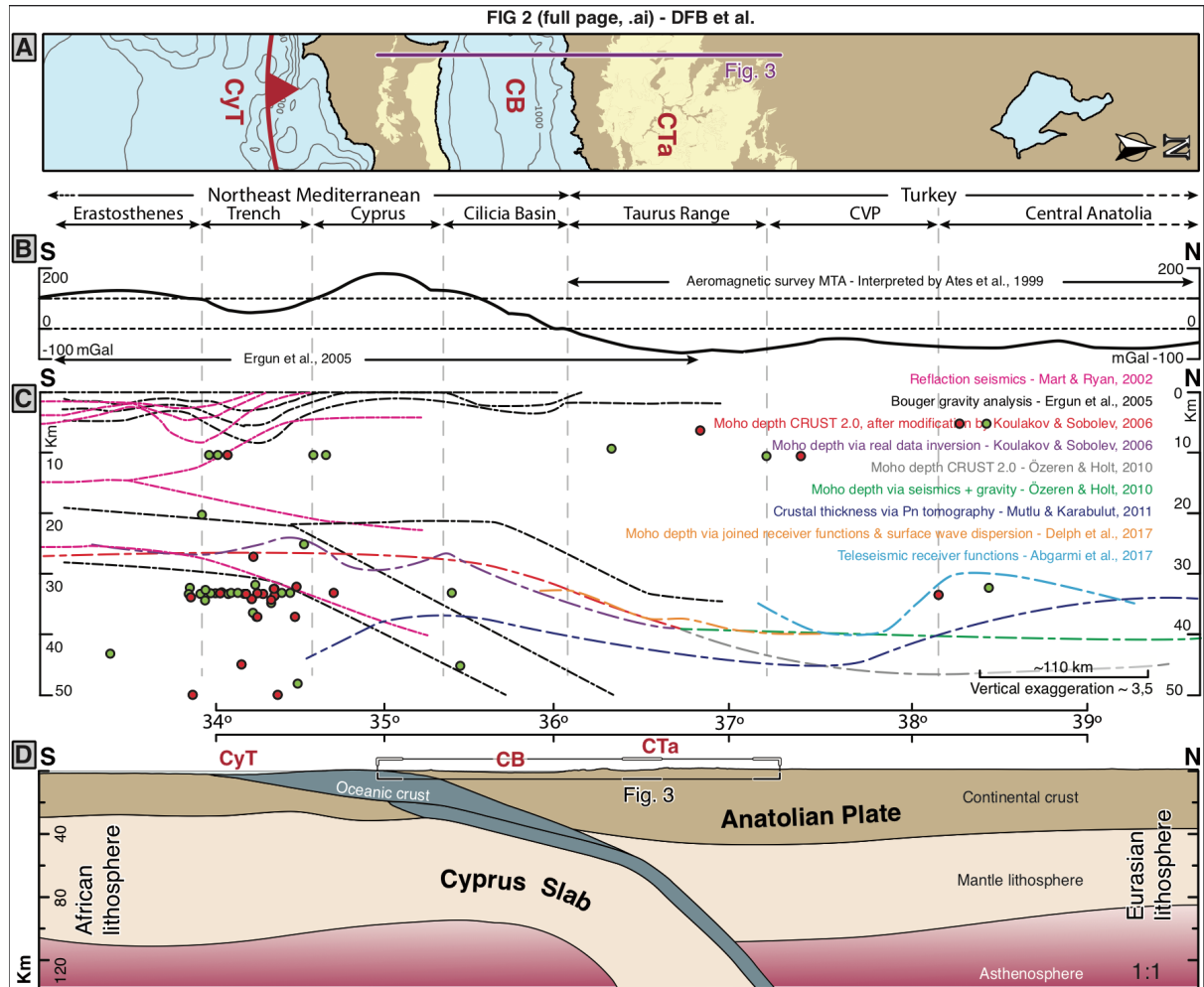


**Figure 2. Plate-scale transect. (A)** Map view of a 2°-longitude wide (32°30' E to 34°30' E) swath running ~650 km along latitude, as a reference for data along transects in panels (B) and (C). **(B)** Values along the section of interest derived from the two major gravimetric studies in the area (Ates et al., 1999; Ergün et al., 2005). **(C)** Published geophysical data, including the interpretation of the offshore section C in Ergün et al. (2005), and that of the seismic study performed by Mart & Ryan (2002). The plot also includes several cross-sectional values retrieved from maps of Moho depth models derived from different geophysical approaches, including Pn tomography and receiver functions (Abgarmi et al., 2017; Delph et al., 2017; Koulakov and Sobolev, 2006; Mutlu and Karabulut 2011; Özeren and Holt, 2010). The circles are focal epicenters with  $M_w > 5$  recorded in a longitudinal area from 32°30' E to 34° E in red and 31°30' E to 34°30' E in green. **(D)** Lithospheric-scale transect along the Central Cyprus subduction (for ~650 km at 33°30' E) at real scale derived from the interpretation of the data shown in (B) and (C).



### **3 The Anatolian margin**

#### **3.1 South Anatolian margin transect: Lithospheric and crustal structure**

We reconstruct a plate-scale transect spanning from the East Mediterranean to the Central Anatolian Plateau interior along 33°30'E longitude (Fig. 2). To portray the lithospheric structure, we integrate constraints from Biryol et al. (2011) and Bakırcı et al. (2012) into the TransMED transect VII (Stephenson et al., 2004). To derive the crustal structure and constrain the thicknesses of the African and Anatolian crust as well as the dip of the Cyprus slab, we collectively interpret data from 10+ geophysical studies along the section (Fig. 2B,-C, see caption).

Along the Central Cyprus subduction zone, the African lithosphere under-thrusts northwards below the Anatolian plate (Fig. 2D). The overriding Anatolian lithosphere has maximum thicknesses of ~110 km at the contact with the Cyprus slab below the modern Central Taurides, and thins northwards down to ~85 km in Central Anatolia (Fig. 2D).

In the southern sectors of the transect, crustal thicknesses are well detected by the gravimetric signal of Ergün et al. (2005) and the Moho models of Koulakov and Sobolev (2006). In the African plate, crustal thicknesses of ~28 km are observed at the site of the Eratosthenes Seamount, south of Cyprus, where the African lithosphere is ~40 km thicker than northwards (Fig. 2D). The oceanic crust is the thinnest (~25 km) below the trench area. Northward and between the subducting and overriding plates, thickening occurs in relation to the Troodos Ophiolite, possibly as a result of thrust doubling due to its emplacement. The locked underthrust of the Eratosthenes Seamount is underneath this location, and the detachment depth of the Troodos Ophiolite is uncertain. Similarly, the extent of the continental crust underneath the Troodos Ophiolite and the position of its transition to oceanic crust farther to the north remains enigmatic. The Anatolian plate has maximum crustal thicknesses of ~45 km (Luccio and Pasyanos, 2007) below the Central Taurides that decrease gently towards the plate interior to ~35 km (Fig. 2D). For this interpretation, we used Pn tomography from Mutlu and

Karabulut (2011) instead of gravity data (Özeren and Holt, 2010), which points to crustal thickness values up to 10 km thicker (Fig. 2C).

All geophysical models concur on a northwards increase in Moho depth from ~28 km to >40 km between 34°30'N and 37°N (Fig. 2C) that we correlate with the steepening of the subducting slab (up to 40°) (Fig. 2D). An overall subduction angle of 45° is observed until ~60 km depth at 36°30', where angles of ~60° are reached as the slab deepens. Northward prolongation at similar dips fit appearances of the slab at ~300 km in the interior of Central Anatolia (A-A section of Biryol et al., 2011).

### **3.2 Central Cyprus forearc transect: Structural and stratigraphic relationships**

We reproduce uppermost crustal structures and the geometry of Miocene and younger rocks (Fig. 3) integrating own findings (Fernández-Blanco, 2014; Fernández-Blanco et al., 2019) with published data in regional studies (e.g., Calon et al., 2005; Robertson, 1998; Stephenson et al., 2004). We assembled the interpretations of each area as shown in their original sources and the reader is referred there for details.

Compressional, regional-scale structures along the Cyprus forearc become older northwards (Fig. 3A). South-verging thrusts rooted in the subduction megathrust are presently active in the trench and pass northwards into thrust culminations covered by Quaternary and Pleistocene rocks in North Cyprus (Fig. 3A-b). The north-verging thrust in Central Cilicia Basin is mid-Pliocene (Fig. 3A-c). In the Cilicia Basin northern margin, Messinian salts pinch out where Pliocene rocks overlay an erosional contact with Miocene rocks, attesting to pre-Pliocene uplift. Uplifted Miocene rocks in the Mut Basin delineate a flexural monocline with no Miocene or younger surface-reaching thrusts (Fig. 3A-d). These regional-scale structures result in structural highs that bound basins or basin sectors and compartmentalize the Cyprus forearc at distances of ~40-50 km (Fig. 3A, a to f). A basement high and the Kyrenia Range bound the Messaoria Basin (a to b, ~40 km), and a deep-rooted thrust system in the center of the Cilicia Basin (Fig. 3A-c) set two sub-basins with similar length (~50 km). Basement highs discriminating sectors

within the Mut Basin (d, e, f in Fig. 3A) also appear at similar distances. These observations are consistent with strain accommodation lead by accretion in the Central Cyprus subduction margin.

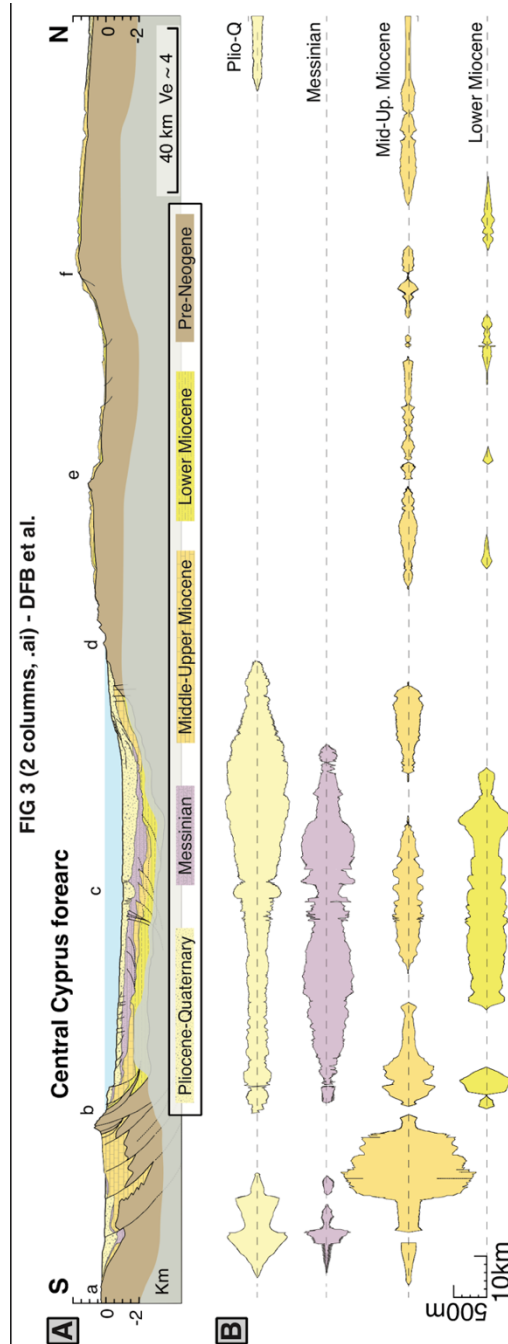


**Figure 3. Uppermost crustal transect. (A)** Geologic transect along the Central Cyprus forearc (for ~300 km at 33°30' E), exaggerated ~4 times in the vertical. Letters “a” to “f” show the approximate location of structural highs bounding basinal sectors with similar lengths. See main text for data used and interpretation. **(B)** Thicknesses of main stratigraphical units derived from the transect and their age.

Basin infill is regionally continuous until the Messinian and deposited exclusively in seaward sectors of the Central Cyprus forearc thereafter (Fig. 3B). After terrestrial sedimentation, pre-Messinian Miocene neritic limestones were deposited atop pre-Miocene basement (Cosentino et al., 2012). These shallow-water rocks are continuous from the Messaoria Basin, where the pre-Messinian basin thins to the south, to Central Turkey. Since the Messinian, rocks deposited seaward off the present Turkish coast and have basin depocenters occurring at northward locations at younger ages (Fig. 3B). This evidence suggests protracted, large-wavelength subsidence of a wide forearc basin prior to the Messinian, followed by younger surface uplift of the modern Central Taurides with concomitant, counteracting subsidence in the Cilicia Basin.

## **4 Thermo-mechanical models of accretion**

Upper-plate strain and morphology at accretionary margins is often described using the critical wedge theory (e.g., Davis et al., 1983), which defines the geometry of the orogenic wedge as a function of the mechanical properties of the accreting wedge. In its strict, brittle form, critical Coulomb wedge theory does not include the ductile properties of these systems. Research inclusive of the visco-plastic attributes show the influence of thermal or rheological variations or that of sediment load and/or competence in the strain distribution and deformation patterns within the accretionary wedge (e.g., Fillon et al., 2013; Fuller et al., 2006; Mannu et al., 2016; Royden, 1996; Vanderhaeghe et al., 2003; Willett and Schlunegger, 2010; Williams et al., 1994).

### **4.1 Model set-up and strategy**

We use a 2D kinematic-dynamic model with standard rheological and thermal parameters to explore feasible mechanisms leading to the present structure of the Anatolian subduction margin (Fig. 4). Models are visco-plastic and similar to those in other studies exploring the evolution of accretionary settings over millions of years (e.g., Fillon et al., 2013; Fuller et al., 2006; Mannu et al., 2016; Royden, 1996; Vanderhaeghe et al., 2003; Willett and Schlunegger,

2010; Williams et al., 1994). Albeit important for shorter-term processes, elasticity is only considered for the flexural isostatic response to vertical loads and included as an elastic foundation that is calculated by assuming two elastic plates that remain in contact (Fuller, 2006). Our models consist of coupled mechanical and thermal domains. The domain where mechanical laws apply represents the crust of a deforming subduction zone where sedimentary accretion of incoming sediments is driven by tangential velocities at its base. Tangential velocities decrease toward, and become zero, at the “S” point, which represents the contact point between the subducting slab and continental Moho (Fig. 4). The thermal domain covers the whole model, including the mechanical domain (Fig. S1). Models simulate the growth of an accretionary wedge at a rate determined by the accretionary flux, as defined by the thickness of accreting material and convergence velocity.

Our simulations aim at being consistent with the time evolution of the Anatolian subduction margin and parameter values are chosen to match plate-scale and upper crustal observations along the transects in Central Cyprus (Figs. 2 & 3) at the end of model run. Models simulate 25 Ma of subduction in a transect of 550 km, with an accretionary thickness  $h = 3$  km and a convergence velocity  $v_c = 35$  mm/yr (Fig. 4), i.e. an accretionary flux of  $105 \text{ km}^2/\text{My}$ , and have a sedimentation rate of  $Sed_r = 0.5$  mm/yr that occurs as the wedge grows until sediments fill depressions to capacity. Models have constant accretionary thickness and convergence velocity that are estimates derived from the extrapolation of present-day values over 25 Ma run time and are lower and higher than present, respectively. Present-day sedimentary thicknesses in the East Mediterranean Sea, ranging from 10 km to 15 km (e.g., Makris and Stobbe, 1984), are the largest in the history of the margin, given the narrower confinement of the modern Mediterranean and the presence of the Nile. Similarly, present-day convergence velocities of  $9.3 \pm 0.3$  mm/yr (Reilinger et al., 2006) are slower than in the recent past due to the underthrusting of the Eratosthenes Seamount below south Cyprus. In general, results scale such that the accretionary flux and run time trade-off at nearly one to one.

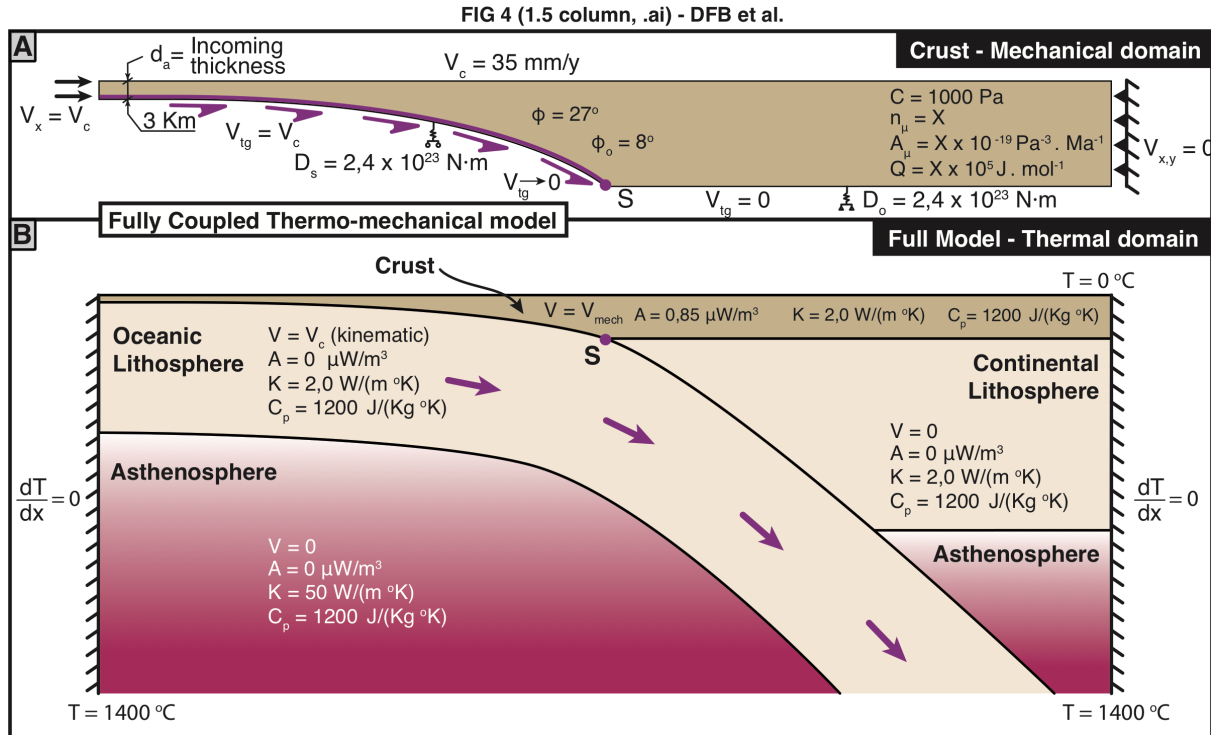


**Figure 4.** Model setup, with an indication of mechanical and thermal parameters.

The subducting lithosphere is 50 My old at the left side of the model and has a thickness of 70 km that remains constant during model run time. Since thicknesses in the mechanical domain change as material is accreted, we chose an initial thickness of 30 km that leads to end-model crustal thicknesses of 45 km near the “S” point, thereby matching the crustal thickness below the Central Taurides. The rest of the overriding lithosphere is 80 km thick. To let the thermal structure equilibrate, the thermal model runs for 20 My before the crustal model onsets. Cohesion and internal friction angles control the mechanical strengths in our model (Fig. 4). Cohesion,  $c$ , is set to 1000 Pa, a value higher than expected for the crust, to maintain model stability. Lower values do not affect the outcomes (Fuller, 2006). The internal friction angle of the crustal material,  $\phi$ , is set to  $27^\circ$  and the friction angle between the subducting and overriding plate,  $\phi_b$ , to  $8^\circ$ . Friction values are set low to include the effect of fluid pressures not explicitly taken into account and imply fluid pressure ratios within the range of those at accretionary wedges (Fuller, 2006, and references therein). Other parameter values are not specific to the Anatolian margin nor to our numerical models and are described in detail in Fuller (2006) and Cassola (2013).

## 4.2 Model results

Model results portray the evolution over millions of years of accreting subduction wedges with forearc highs, and show the typical morphologic elements of these systems (Fig. 5 & Video S2). North of the seaward migrating trench, the trench-slope wedge bounds a wide topographic depression that grows continuously as accommodation space is created by the landward increasing depth of the subduction slab. Steady infill of the forearc depression suppresses strain rates and deformation of the underlying wedge, providing the stability to maintain an undeformed sedimentary basin in a negative-alpha setting (Fig. 5B). Temperature increases under the basin during its growth leading to a viscosity drop in the lower crust and ductile strain that ultimately results in uplift of the forearc high and subsidence at seaward locations (Fig. 5C). At the end of the model run, subduction wedge accretion has led to elevated strain rates and widespread deformation from the trench to the forearc high. Subduction wedge accretion also results in wedge topography and wedge thickness continuously increasing landward until the forearc high, where topographic height is maximum.

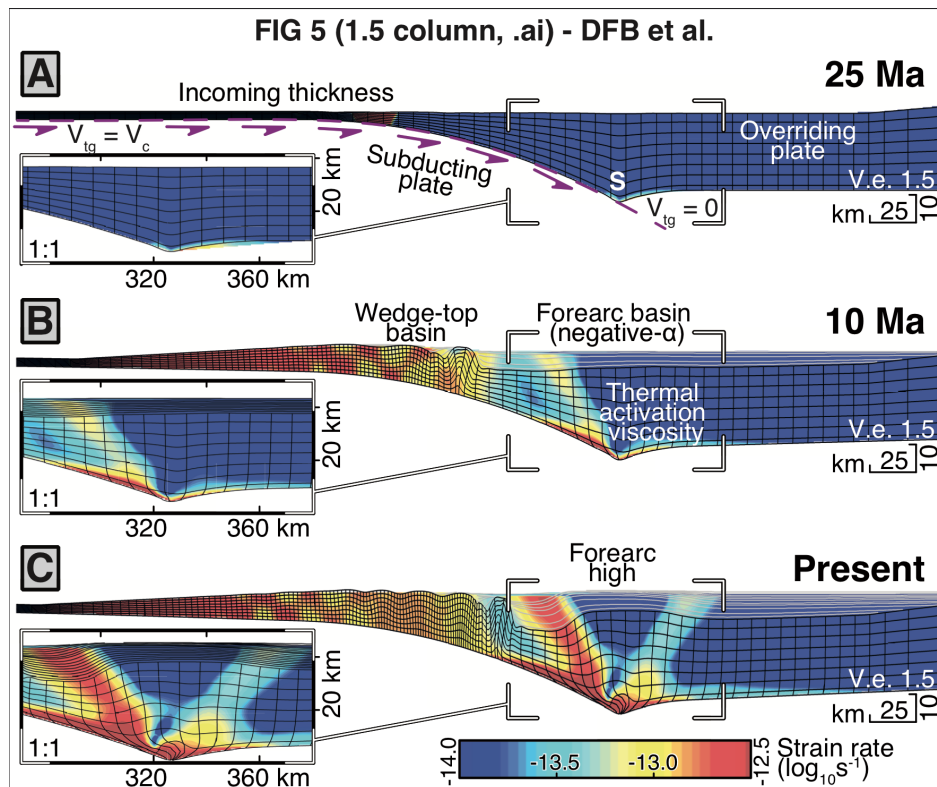


**Figure 5.** Three time-steps (initiation, ~10 Ma and present) in the numerical thermo-mechanical model of viscous-plastic deformation for a convergent wedge undergoing basal traction to simulate subduction (see DR3). Insets are zoom-ins of the area where the forearc high develops at the model scale. The color shows the second invariant of strain rate tensor, i.e. strain rate. The cumulative strain is shown by the Lagrangian mesh. Individual lines on top of the basement are isochrones (synthetic stratigraphy) that reflect the overall geometric relationships expected for strata. The upper panel represents the moment of subduction initiation at 25 Ma. The middle panel at 10 Ma shows a wide forearc (negative- $\alpha$ ) basin, increase in strain rate below it and wedge deformation reaching the future location of the forearc high. The bottom panel at present shows a forearc high developed by a wide shear zone and onlaps in the synthetic stratigraphy above large strain rates at the lower crust. The model does not include erosion, so sediments draping the forearc high are still present, but would be expected to erode quickly, were this process included. See video Video S1 in Supplementary Material.

#### **4.2.1 Sedimentation and forearc high uplift**

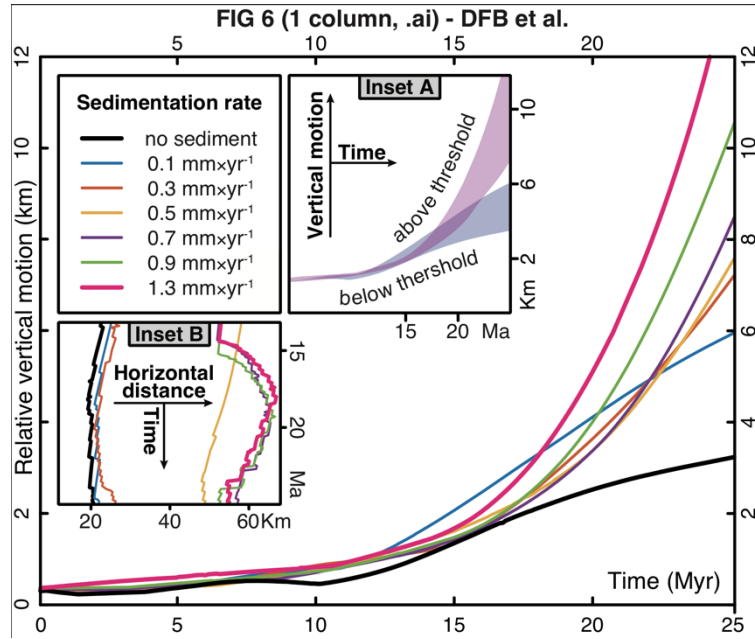
Sedimentation rates in the forearc basin fundamentally affect vertical motions in the forearc high at advanced stages of wedge evolution. To explore this effect, we plot how models with different sedimentation rates (0 to 1.3 mm/yr) change the time evolution of relative vertical motion between the highest and lowest point of the forearc basement (Fig. 6). At early stages of wedge evolution (15 Ma model run time), variations in sedimentation rate have minimum effect in forearc topography with relative vertical motions that have constant rates of ~0.04-0.05 mm/yr. Thereon, sedimentation rates above and below a threshold value result in two different trends in the rate of change of relative vertical motions (Fig. 6, Inset A); whereas lower, below-threshold sedimentation rates (<0.3 mm/yr) lead to convex-up trends in the time evolution of relative vertical motions, concave-up trends occur with higher, above-threshold sedimentation rates (0.3 mm/yr and higher). Below-threshold sedimentation rates result in rates of relative vertical motion of ~0.2-0.4 mm/yr (black and blue in Fig. 6). Above-threshold sedimentation rates lead to relative vertical motion rates ranging from ~0.72 mm/yr to ~1.75 mm/yr as sedimentation rate changes from 0.3 mm/yr to 1.3 mm/yr, respectively (orange to magenta in Fig. 6).



We also track the horizontal distance between the highest and lowest point of the forearc basement during the last stages of model run, i.e. the period of differentiation in vertical motions as led by sedimentation (Fig. 6, Inset B). For all simulations, the horizontal distance between the highest point on the forearc high and the lowest point on its depocenter is short (<70 km) with regards to its associated vertical motion (up to >12 km). Such horizontal distance is also controlled by a threshold value in sedimentation rate (Fig. 6, Inset B); whereas models with lower sedimentation rates lead to horizontal distances of ~20 km that are consistent throughout the model run, those with higher sedimentation rates show horizontal distances between 40 km and 70 km that vary during the model run. For the latter simulations, once vertical motions onset, horizontal distances for the tracked points increase suddenly for a period of ~3 Ma and decrease thereon for the rest of the model run (Fig. 6, Inset B). These changes in horizontal distance reflect the steepening in time of the transitional area between uplifting and subsiding areas.

The aforementioned non-linear relation between sedimentation rates and forearc high growth controlled by a threshold value suggest the activation of an external forcing that contributes to vertical motions in the interior of mature wedges. Below, we evaluate whether such external forcing is forearc basin sedimentation leading to thermally-activated deformation and viscous flow at the base of the crust. This evaluation also provides information on the sensitivity to variations of sedimentation rate regarding this sediment “blanketing” effect.

**Figure 6.** *Sedimentation rate influence on the time evolution of vertical motions in a forearc high. Each colored line shows the height difference between the highest and lowest basement elevation in a 100 km strip centered around the S point and above it. A total of 250 height-difference data points (one every  $10^5$  yr) compound each line of sedimentation rate, from a simulation with no sedimentation rate (black) to rates of 1.3 mm/yr (magenta). Inset A is a schematic representation of vertical motions in time for the groups below and above the threshold in sedimentation rates. Inset B is the evolution in time of the horizontal distance between the highest and the lowest point in the basement surface for the last 12 Ma of model run.*



#### 4.2.2 Sediment blanketing controls on temperature and viscosity

We derive the evolution in time of temperature and viscosity (Fig. 7) using all model grid elements located in the mechanical domain within a 200 km box centred in the S-point (boxes of Fig. 5 insets). We plot single values of median temperature (Fig. 6A) and median viscosity (Fig. 6B) for 250 model snapshots (every  $10^5$  yr) for simulations with sedimentation rates ranging from 0.1 mm/yr to 0.9 mm/yr. To assure a representative, non-parametric calculus, we use the median for both temperature field and viscosity distribution. For the former, we compute median temperature values for each grid point, thereby avoiding potential complications related to multi-modal distributions in temperature fields of geodynamic models. For the latter, we compute the median viscosity of highly-strained regions (shear zones). To avoid the tendency of average values to misrepresent power-law distributions, we calculate the strain rates for all grid elements and use the median viscosity of the 10% with larger strain rates.

The amount of wedge-top sediments control the vertical gradient of temperature and the evolution of viscosity in the underlying wedge (Fig. 7). Models reveal a transition at  $\sim 15$  Ma, when the same wedge temperature is recorded for all models, regardless of their sedimentation rate. Models with higher sedimentation rates decrease the overall wedge temperature before the transition and increase it after the transition, with respect to lower sedimentation rate

models (Fig. 7A). As sedimentation rate increases, temperature variations become not linear and are twice as large in the advance stages of wedge evolution, with models varying sedimentation rate from 0.1 mm/yr to 0.9 mm/yr resulting in a temperature change of  $-10^{\circ}\text{C}$  in before the transition and  $+30^{\circ}\text{C}$  degrees after it. This change in wedge temperature with increased sedimentation rates and the aforementioned transition are also observed in the evolution of viscosity in shear zones (Fig. 7B). Whereas lower sedimentation rate models have the lowest values of viscosity in shear zones for early times of model run, higher sedimentation rate models record the lowest values of viscosity at advanced stages (Fig. 7B).

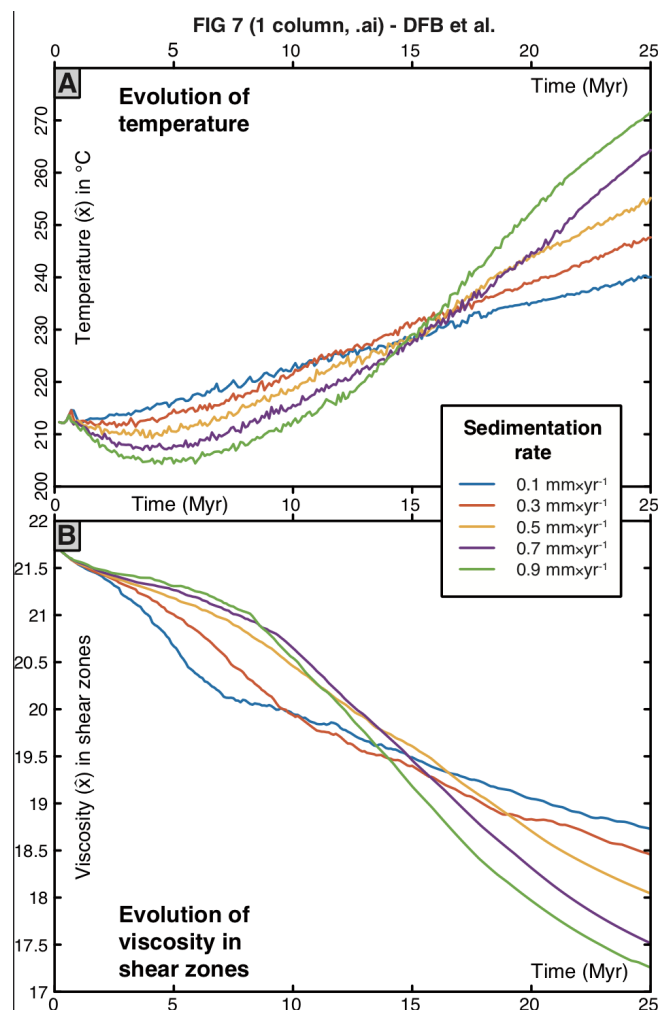


**Figure 7.** Evolution of median temperature (A) and median viscosity in shear zones (B) for models with different sedimentation rate, calculated every 100 kyr (250 snapshots). Different line colors represent sedimentation rates of 0.1 mm/yr (blue), 0.3 mm/yr (red), 0.5 mm/yr (yellow), 0.7 mm/yr (purple), and 0.9 mm/yr (green).

Sedimentation rates control the growth of a forearc high in mature accretionary wedges, and the rate of associated topographic growth, ultimately leading to regional vertical motions of opposite sense and short wavelength (Fig. 6). The correlation of increased sedimentation rates with larger relative vertical motions in the forearc high as well as with increased temperatures and lower viscosity below it (Fig. 7) strongly support that sediments have a “thermal blanketing” effect that induces viscous flow in the lower crust and the uplift of the forearc high. Thermal resistivity of sediments leads to “thermal blanketing” and increasingly higher temperatures in the underlying wedge as the basin grows, and ultimately results in the progressive change in the deformation mechanism from Coulomb friction to nonlinear viscous at the base of the crust (Figs. 5B & 7). Lowering strength results in viscous flow at the base of the orogen and, given the compressional state of the wedge, it shortens horizontally and thickens, uplifting the forearc high (Fig. 5C). Thus, the forearc basin “thermal blanket” promotes deep-seated deformation that, in the context of accretion, propels the uplift of the forearc high while subsidence continues in seaward regions that are unaffected by viscous flow (Figs. 5, 6 & 7).

## **4 Discussion**

Deep-seated flow (Pavlis and Bruhn, 1983) at the base of an orogenic wedge (Platt, 1986; Willett et al., 1993) provides a simple general framework to explain the dynamic formation of forearc highs. Crustal thickening by protracted wedge accretion increases the depth of burial and the temperature of the lower crust (Willett et al., 1993). Synorogenic sedimentation filling a forearc basin similarly contributes to wedge thickening, and also raises lower crustal temperatures by increasing thermal resistance and, if sediment conductivity is low, the geothermal gradient through the basin (Fuller et al., 2006).

### **5.1 Dynamic growth of forearc highs**

The fundamental conditions required by the model presented here are quite simple. Accretion

and syn-accretion sedimentation result in a progressive increase of crustal thickness in a subduction margin forearc. The increased thickness increases thermal resistance and Moho depth, thereby increasing lower crustal temperatures and changing deformation from frictional to viscous. Under protracted accretion and shortening, ductile strain in the lower crust switches vertical tectonic motions in the overlying wedge, from forearc basin subsidence to uplift, forming a new forearc high directly under the former basin (Fig. 8). We expect this process to take place in any accretionary system as it matures and increases in size, as for example documented on the Cascadia margin (Fuller et al., 2006; McNeill et al., 2000).

A viscous-flow controlled, structurally internal forearc high as we propose will form at a location determined by the geometry of the slab, as integral parts of accretionary wedges that uplift in a dynamic, non-linear manner. In this context, forearc highs become more probable as the accretion system matures and form at a time dictated by accretionary flux, wedge temperature, and wedge viscosity. We note, however, that there are other mechanisms for the formation of a forearc high, including forced mechanical accretion against areas of relatively larger strength (Byrne et al., 1993), changes in wedge taper or stress state (Willett & Schlunegger, 2010), or other processes leading to deep-seated ductility (Pavlis and Bruhn, 1983), such as the presence of fluids.

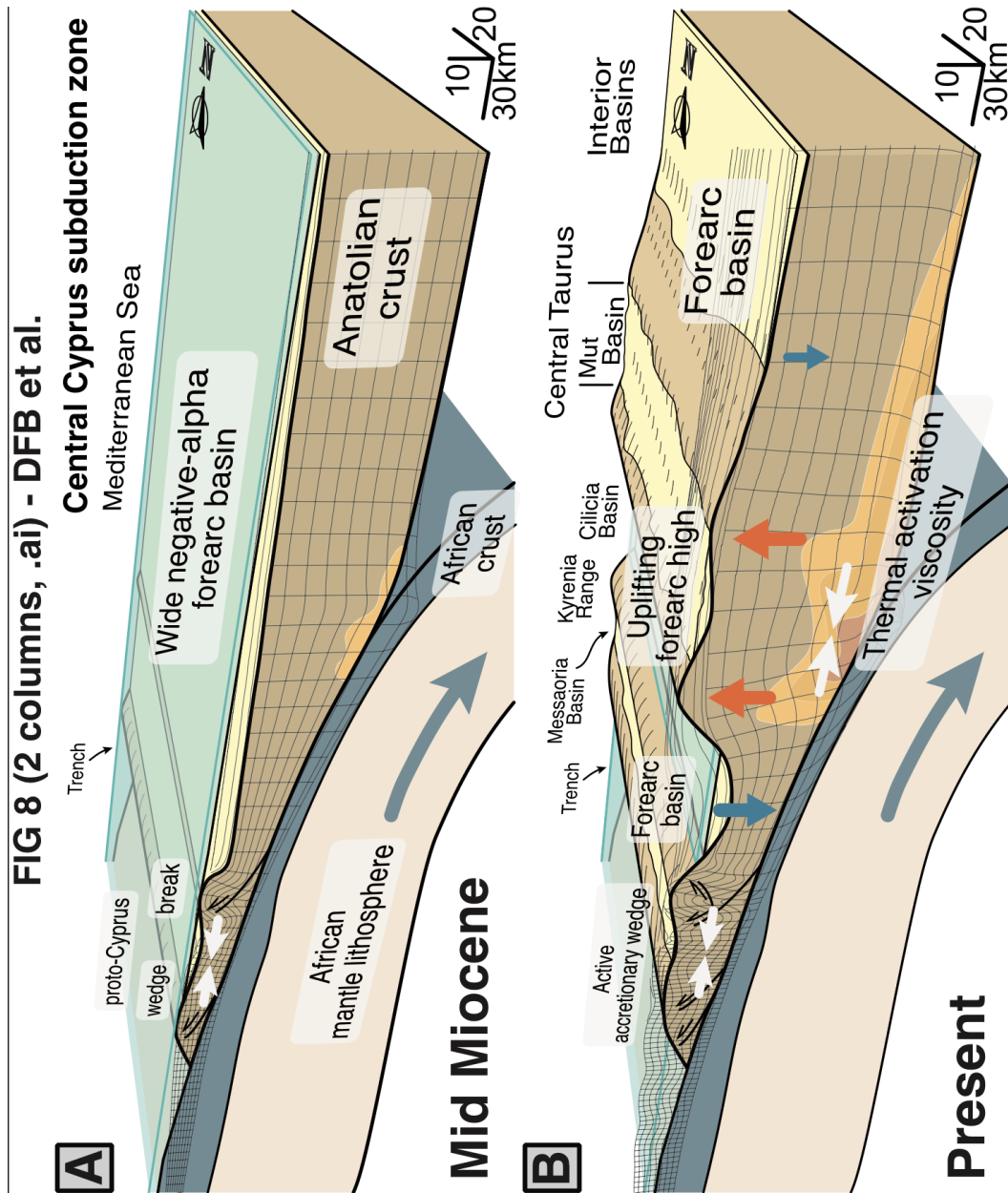
Competing, dynamic effects control the uplift of the forearc high. Synorogenic sedimentation increases the thermal resistance and thus temperature of the underlying crust. If sediments have a low thermal conductivity, this effect is even more pronounced. While a weaker lower crust tends to decrease the wedge taper, it also facilitates ductile strain that, when sustained by accretion, results in increasing the wedge taper. Therefore, the taper geometry of the internal sectors of the wedge depends not only on convergence velocity (Willett et al., 1993) but also on its interplay with forearc basin sedimentation. The area undergoing lower crustal flow generates uplift in regions immediately above it, while trenchward regions not affected by lower crustal flow continue to subside through sediment loading. The transitional area from forearc high to trenchward subsidence is regarded as ductile-to-frictional decollement in

Williams et al., (1994) and as decoupled-to-coupled flow in Royden (1996).

Sedimentation controls the lag time between wedge growth and thermal activation of lower crustal flow. Whereas no relevant topographic growth occurs in the internal sectors of the wedge during its early evolution, regardless of the amount of sediments in the forearc, a threshold in the amount of sediment in the forearc controls the growth of the forearc high at advanced stages of wedge (Figs. 6, 7 & 8). This implies that the lower crustal flow is controlled by the thickness of the crust, which depends in turn on the sedimentation rates in the forearc basin. In other words, the sedimentary blanketing effect controls the lower crustal flow in so that the drop in viscosity does not occur until sediment thickness reaches a threshold. Otherwise, crustal thickening alone would eventually lead to viscous deformation, albeit occurring later and possibly elsewhere in the mechanical system.

Sedimentation and sedimentation rate have other effects that control forearc high uplift. Sediment infill of the forearc topographic depression reduces the surface angle of the forearc wedge to zero and stabilizes the wedge underneath, resulting in a broad wedge where active deformation is confined to an outer wedge removed from any material-controlled backstop (Fuller et al., 2006). In addition, isostatic basin subsidence by sediment loading of the forearc persists seaward and landward of the uplifting forearc high. This leads to the apparent paradox that regional subsidence in the forearc basin can control uplift in the forearc high for cases where sedimentation rate outpaces accommodation space, i.e. when subsidence controls the amount of sediment entering the system.

**Figure 8.** Box model representation of the mechanism of thermo-viscous forearc high uplift in two time-steps. Boxes show the evolution and forearc elements for a generic subduction wedge with forearc high and for the Central Cyprus margin. Time steps are interpreted as representative of the Central Cyprus margin. Integrated deformation is shown using the Lagrangian mesh of the model. Note that the model is only two-dimensional.



## 5.2 Growth of the Anatolian margin

Our simulations are consistent with SCAP formation as a dynamic, thermo-viscous forearc high led by forearc sedimentation and accretion along Central Cyprus (Fig. 8). Models reproduce the growth of the SCAP, including the surface uplift of Central Taurus and coeval subsidence in the Cilicia Basin, resulting in the monoclinial flexure of Late Miocene rocks at the plateau margin scale (Fernández-Blanco et al., 2019) (Figs. 3 & 8). This is compatible with surface uplift onset between 8 and 5.45 Ma in the plateau margin hinterland (Cosentino et al., 2012), and a well-developed orogenic rain shadow by 5 Ma (Meijers et al., 2018) as well as the concomitant, short-

wavelength vertical tectonic motions described for S Turkey (Fernández-Blanco et al., 2019; Walsh-Kennedy et al., 2014). Models are also coherent with strong observational evidence like the undisrupted and copious sedimentary record in the SCAP offshore through the latest Messinian - Recent times (Aksu et al., 2014, 2005; Walsh-Kennedy et al., 2014). Therefore, the mechanism of dynamic, thermo-viscous forearc high growth provides a physical support for models of SCAP growth by contraction and crustal thickening (Fernández-Blanco, 2014; Fernández-Blanco et al., 2019; Meijers et al., 2018).

Accelerated uplift rates during the uplift of the Central Taurides forearc can be inferred from the elevations of Miocene to Pleistocene marine rocks. These rocks show that the onset of uplift initiated at ~8 Ma (Cosentino et al., 2012) and accelerated to ~0.75 mm/yr over the last ~1.6 Ma (Schildgen et al., 2012). Our models show the occurrence of an equivalent accelerated uplift as a natural consequence of the non-linear uplift associated with thermal weakening of the lower crust (Fig. 5B,-C, 6, 7, 8B). Most observations of uplift rates are consistent with our models, but one study has suggested that 1200-1500 m of topographic growth occurred within the last ~450 ka (Öğretmen et al., 2018). The spatial location of the marine deposits analysed by this study is relatively local, but if applicable to the entire margin would be difficult to reconcile with our models.

Primary alternative models for uplift of the Taurides forearc high suggest shallow slab break-off and multiple-phase surface uplift (e.g., Schildgen et al., 2014). However, slab break-off models do not inherently predict extended periods of uplift or accelerated uplift, so the earlier uplift during the Miocene has been attributed to structural thickening, similar to what we predict here (Schildgen et al., 2014) with the high rates of uplift associated with slab break-off in the last ~1.6 Ma (Schildgen et al., 2012) or younger times (Öğretmen et al., 2018). Slab break-off is an independent process to lower crustal viscous flow and it is possible that both have occurred and contribute to the uplift of S Turkey. However, our models show that there are combinations of parameters that predict growth rates, timing and accelerations consistent with the observations, with no need for an additional mechanism such as slab break-off.



Schildgen et al. (2012) argued that uplift rates exhibited a rapid increase in rate initiating at about  $\sim 1.6$  Ma, on the basis of analysis of knickpoints in rivers draining the Central Taurides. However, the river knickpoints are not particularly uniform in their elevation or along-channel distribution, and could be consistent with a gradual increase in uplift rate from Late Miocene to the present, particularly if other complicating factors such as tilting and river capture are taken into account. Similarly, these studies interpret the depositional age or subaerial exposure of marine rocks at individual sites in terms of uplift age and uplift spatiotemporal pattern, i.e. temporal phases of uplift at margin scale. However, the uplifted marine sediment data cannot resolve sharp changes in uplift rate and only show that rates averaged over the Pliocene and Late Miocene were lower than rates over the Pleistocene to modern.

Our models show that compression-driven wedge growth with sedimentation can not only provide an uplift mechanism for the southern margin of the Central Anatolian Plateau but also reproduce first-order upper plate strain and the complex geometry and patterns of vertical motion in space and time that characterize the southern Anatolian margin (Figs. 3 & 8). These simulations agree with the regional frame and the geological and geophysical observables in the Anatolian margin along the Central Cyprus subduction zone, including in and under the area undergoing maximum uplift. The Kyrenia Range trench-slope break divides the active frictional deformation in the seaward areas, resulting in wedge top basin of Messaoria, from the negative-alpha Cilicia Basin, and from areas farther landward where thermally-activated viscosity in the deeper sectors of the wedge resulted in the uplift of the modern Central Taurides (Figs. 3, 5 & 8). Our simulations could reproduce the dynamic growth of wider plateau-like terrains, but the mechanism presented here cannot be responsible for the topography of the entire Central Anatolian Plateau, given the thin crust in the plateau interior (e.g., Abgarmi et al., 2017). This mechanism is also compatible with disruption of the former forearc basin by uplift of the forearc high in Cascadia (McNeill et al., 2000), and suggests similar processes in the Alaskan and Nankai accretionary margins (Pavlis and Bruhn, 1983).

## **6 Conclusions**

Integration and interpretation of geophysical and geological evidence along the Anatolian subduction margin from the Central Cyprus trench to the SCAP suggests that lithospheric and crustal thicknesses, as well as Miocene and younger regional-scale structures and derived tectono-stratigraphic features formed by accretionary subduction. In this context, thermally-activated viscous flow of the lower crust is a physical mechanism of forearc high growth.

Thermo-mechanical models of this process show that this single mechanism can explain much of the complex space and time pattern of vertical motions in the Anatolian subduction margin, with no need for an additional mechanism such as slab breakoff. We conclude that the plateau margin in South Turkey, and areas with a similar sequence of vertical motions in the interior of other accreting subduction wedges, grow as dynamic, thermo-viscous forearc highs.

## **Acknowledgments**

The authors want to thank three anonymous reviewers for their constructive criticisms. We thank the Netherlands Organisation for Scientific Research (NWO) for founding this study as a part of the Vertical Anatolian Movement Project (VAMP), an European Science Foundation (ESF) EuroCORE project within TOPOEurope. Grant/Award Number: 855.01.142 (07-TOPO-EUROPE-FP-013) Miocene tectonics in the Central Anatolia Plateau, and the Netherlands Organisation for Scientific Research. DFB thanks Teodoro Cassola for his guidance with the models, and Melodie Philippon and Christoph von Hagke for discussions.

## References

- Abgarmi, B., Delph, J.R., Arda Ozacar, A., Beck, S.L., Zandt, G., Sandvol, E., Turkelli, N., Berk Biryol, C., 2017. Structure of the crust and African slab beneath the central Anatolian plateau from receiver functions: New insights on isostatic compensation and slab dynamics. *Geosphere* 13, 1774–1787.
- Aksu, A.E., Calon, T.J., Hall, J., Mansfield, S., Yaşar, D., 2005. The Cilicia–Adana basin complex, Eastern Mediterranean: Neogene evolution of an active fore-arc basin in an obliquely convergent margin. *Marine Geology* 221, 121–159.
- Aksu, A.E., Walsh-Kennedy, S., Hall, J., Hiscott, R.N., Yaltırak, C., Akhun, S.D., Çifçi, G., 2014. The Pliocene–Quaternary tectonic evolution of the Cilicia and Adana basins, eastern Mediterranean: Special reference to the development of the Kozan Fault zone. *Tectonophysics* 622, 22–43.
- Allmendinger, R., Jordan, T., Kay, S., Isacks, B., 1997. The evolution of the Altiplano-Puna plateau of the Central Andes. *Annual Review of Earth and Planetary Sciences* 25, 139–174.
- Ates, A., Kearey, P., Tufan, S., 1999. New gravity and magnetic anomaly maps of Turkey. *Geophys. J. Int.* 136, 499–502.
- Bakırcı, T., Yoshizawa, K., Özer, M., 2012. Three-dimensional S-wave structure of the upper mantle beneath Turkey from surface wave tomography. *Geophysical Journal International* 190, 1058–1076.
- Bartol, J., Govers, R., 2014. A single cause for uplift of the Central and Eastern Anatolian plateau? *Tectonophysics* 637, 116–136.
- Bassant, P., Van Buchem, F.S.P., Strasser, A., Görür, N., 2005. The stratigraphic architecture and evolution of the Burdigalian carbonate—siliciclastic sedimentary systems of the Mut Basin, Turkey. *Sedimentary Geology* 173, 187–232.
- Biryol, C., Beck, S.L., Zandt, G., Özacar, A., 2011. Segmented African lithosphere beneath the Anatolian region inferred from teleseismic P-wave tomography. *Geophysical Journal International* 184, 1037–1057.
- Byrne, D.E., Wang, W.-H., Davis, D.M., 1993. Mechanical role of backstops in the growth of forearcs. *Tectonics* 12, 123–144.
- Calon, T.J., Aksu, A.E., Hall, J., 2005. The Oligocene–Recent evolution of the Mesaoria Basin (Cyprus) and its western marine extension, Eastern Mediterranean. *Marine Geology* 221, 95–120.
- Cassola, T., 2013. Mechanics of forearc basins. ETH Zurich.
- Cosentino, D., Schildgen, T., Cipollari, P., Faranda, C., Gliozzi, E., Hudáčková, N., Lucifora, S., Strecker, M.R., 2012. Late Miocene surface uplift of the southern margin of the Central Anatolian Plateau, Central Taurides, Turkey. *Geological Society of America Bulletin* 124, 133–145.
- Davis, D., Suppe, J., Dahlen, F.A., 1983. Mechanics of fold-and-thrust belts and accretionary wedges. *Journal of Geophysical Research*.
- Delph, J.R., Abgarmi, B., Ward, K.M., Beck, S.L., Arda Özacar, A., Zandt, G., Sandvol, E., Türkelli, N., Kalafat, D., 2017. The effects of subduction termination on the continental lithosphere: Linking volcanism, deformation, surface uplift, and slab tearing in central Anatolia. *Geosphere* 13, 1788–1805.
- Ergün, M., Okay, S., Sari, C., Zafer Oral, E., Ash, M., Hall, J., Miller, H., 2005. Gravity anomalies of the Cyprus Arc and their tectonic implications. *Marine Geology* 221, 349–358.
- Fernández-Blanco, D., 2014. Evolution of Orogenic Plateaus at Subduction Zones: Sinking and raising the southern margin of the Central Anatolian Plateau.
- Fernández-Blanco, D., Bertotti, G., Aksu, A., Hall, J., 2019. Monoclinical flexure of an orogenic plateau margin during subduction, south Turkey. *Basin Res.* 13, 1774.
- Fillon, C., Huismans, R.S., van der Beek, P., 2013. Syntectonic sedimentation effects on the growth of fold-and-thrust belts. *Geology* 41, 83–86.
- Fuller, C.W., 2006. Controls on the Structural Morphology and Subduction-thrust Seismicity of Accretionary Margins. University of Washington.
- Fuller, C.W., Willett, S.D., Brandon, M.T., 2006. Formation of forearc basins and their influence on subduction zone earthquakes. *Geology* 34, 65–68.
- Göğüş, O.H., Pysklywec, R.N., 2008. Mantle lithosphere delamination driving plateau uplift and synconvergent extension in eastern Anatolia. *Geology* 36, 723–726.
- Göğüş, O.H., Pysklywec, R.N., Şengör, A.M.C., Gün, E., 2017. Drip tectonics and the enigmatic uplift of the Central Anatolian Plateau. *Nature Communications* 8, 1538.
- Karabiyiçoğlu, M., Çiner, A., Monod, O., Deynoux, M., Tuzcu, S., and Örcen, S., 2000. Tectonosedimentary evolution of the Miocene Manavgat Basin, western Taurides, Turkey. *Geological Society, London, Special Publications* 137, 271–294.

- Koulakov, I., Sobolev, S.V., 2006. Moho depth and three-dimensional P and S structure of the crust and uppermost mantle in the Eastern Mediterranean and Middle East derived from tomographic inversion of local ISC data. *Geophys. J. Int.* 164, 218–235.
- Luccio, F., Pasyanos, M.E., 2007. Crustal and upper-mantle structure in the Eastern Mediterranean from the analysis of surface wave dispersion curves. *Geophys. J. Int.* 169, 1139–1152.
- Makris, J., Stobbe, C., 1984. Physical properties and state of the crust and upper mantle of the Eastern Mediterranean Sea deduced from geophysical data. *Marine Geology* 55, 347–363.
- Mannu, U., Ueda, K., Willett, S.D., Gerya, T.V., Strasser, M., 2016. Impact of sedimentation on evolution of accretionary wedges: Insights from high-resolution thermomechanical modeling. *Tectonics* 35, 2016TC004239.
- Mart, Y., Ryan, W.B.F., 2002. The complex tectonic regime of Cyprus arc: a short review. *Isr. J. Earth Sci.* 51, 117–134.
- McNeill, L.C., Goldfinger, C., Kulm, L.D., Yeats, R.S., 2000. Tectonics of the Neogene Cascadia forearc basin: Investigations of a deformed late Miocene unconformity. *GSA Bulletin* 112, 1209–1224.
- Meijers, M.J.M., Brocard, G.Y., Cosca, M.A., Lüdecke, T., Teyssier, C., Whitney, D.L., Mulch, A., 2018. Rapid late Miocene surface uplift of the Central Anatolian Plateau margin. *Earth and Planetary Science Letters* 497, 29–41.
- Molnar, P., 1984. Structure and Tectonics of the Himalaya: Constraints and Implications of Geophysical Data. *Annual Review of Earth and Planetary Sciences* 12, 489–516.
- Mutlu, A.K., Karabulut, H., 2011. Anisotropic Pn tomography of Turkey and adjacent regions. *Geophys. J. Int.* 187, 1743–1758.
- Öğretmen, N., Cipollari, P., Frezza, V., Faranda, C., Karanika, K., Gliozzi, E., Radeff, G., Cosentino, D., 2018. Evidence for 1.5 km of uplift of the Central Anatolian Plateau's southern margin in the last 450 kyr and implications for its multi-phased uplift history. *Tectonics* 2017TC004805.
- Özeren, M.S., Holt, W.E., 2010. The dynamics of the eastern Mediterranean and eastern Turkey. *Geophys. J. Int.* 183, 1165–1184.
- Pavlis, T.L., Bruhn, R.L., 1983. Deep-seated flow as a mechanism for the uplift of broad forearc ridges and its role in the exposure of high P/T metamorphic terranes. *Tectonics* 2, 473–497.
- Platt, J.P., 1986. Dynamics of orogenic wedges and the uplift of high-pressure metamorphic rocks. *GSA Bulletin* 97, 1037–1053.
- Reilinger, R., McClusky, S., Vernant, P., Lawrence, S., Ergintav, S., Cakmak, R., Ozener, H., Kadirov, F., Guliev, I., Stepanyan, R., Nadariya, M., Hahubia, G., Mahmoud, S., Sakr, K., ArRajehi, A., Paradissis, D., Al-Aydrus, A., Prilepin, M., Guseva, T., Evren, E., Dmitrotsa, A., Filikov, S.V., Gomez, F., Al-Ghazzi, R., Karam, G., 2006. GPS constraints on continental deformation in the Africa-Arabia-Eurasia continental collision zone and implications for the dynamics of plate interactions: Eastern Mediterranean active tectonics. *Journal of Geophysical Research, Geodyn. Ser.* 111. <https://doi.org/10.1029/2005JB004051>
- Robertson, A.H.F., 1998. Mesozoic-Tertiary tectonic evolution of the easternmost Mediterranean area: integration of marine and land evidence. *Proceedings of the Ocean Drilling Program, Scientific Results, Vol. 160; Chapter 54.*
- Royden, L., 1996. Coupling and decoupling of crust and mantle in convergent orogens: Implications for strain partitioning in the crust. *J. Geophys. Res., Philos. Trans. R. Soc. London A* 101, 17679–17705.
- Schildgen, T.F., Cosentino, D., Bookhagen, B., Niedermann, S., Yildirim, C., Echtler, H., Wittmann, H., Strecker, M.R., 2012. Multi-phased uplift of the southern margin of the Central Anatolian plateau, Turkey: A record of tectonic and upper mantle processes. *Earth and Planetary Science Letters* 317–318, 85–95.
- Schildgen, T.F., Yildirim, C., Cosentino, D., Strecker, M.R., 2014. Linking slab break-off, Hellenic trench retreat, and uplift of the Central and Eastern Anatolian plateaus. *Earth-Science Reviews* 128, 147–168.
- Stephenson, R.A., Mart, Y., Okay, A., Robertson, A., Saintot, A., Stovba, S., Khriachtchevskaia, O., 2004. TRANSMED Transect VIII: Eastern European Craton--Crimea--Black Sea--Anatolia--Cyprus--Levant Sea--Sinai--Red Sea. *The TRANSMED Atlas: The Mediterranean Region from Crust to Mantle* 120–127.
- Vanderhaeghe, O., Medvedev, S., Fullsack, P., Beaumont, C., Jamieson, R.A., 2003. Evolution of orogenic wedges and continental plateaus: insights from crustal thermal–mechanical models overlying subducting mantle lithosphere. *Geophys. J. Int.* 153, 27–51.
- Walsh-Kennedy, S., Aksu, A.E., Hall, J., Hiscott, R.N., Yaltırak, C., Çifçi, G., 2014. Source to sink: The development of the latest Messinian to Pliocene–Quaternary Cilicia and Adana Basins and their linkages with the onland Mut Basin, eastern Mediterranean. *Tectonophysics* 622, 1–21.

- Willett, S., Beaumont, C., Fullsack, P., 1993. Mechanical model for the tectonics of doubly vergent compressional orogens. *Geology* 21, 371–374.
- Willett, S.D., Schlunegger, F., 2010. The last phase of deposition in the Swiss Molasse Basin: from foredeep to negative-alpha basin. *Basin Research* 22, 623–639.
- Williams, C.A., Connors, C., Dahlen, F.A., Price, E.J., Suppe, J., 1994. Effect of the Brittle-Ductile Transition on the Topography of Compressive Mountain Belts on Earth and Venus. *Journal of Geophysical Research-Solid Earth* 99, 19947–19974.
- Wortel, M., Spakman, W., 2000. Subduction and slab detachment in the Mediterranean-Carpathian region. *Science* 290, 1910–1917.
- Yildirim, C., Schildgen, T.F., Echtler, H., Melnick, D., Strecker, M.R., 2011. Late Neogene and active orogenic uplift in the Central Pontides associated with the North Anatolian Fault: Implications for the northern margin of the Central Anatolian Plateau, Turkey. *Tectonics* 30, TC5005.